Cement and Concrete Research xxx (xxxx) xxx–xxx

Contents lists available at ScienceDirect

Cement and Concrete Research

journal homepage: www.elsevier.com/locate/cemconres

Monitoring the internal swelling in cementitious mortars with single-sided ^{1}H nuclear magnetic resonance

Robert Schulte Holthausen*, Michael Raupach

Institute for Building Material Research (ibac) at RWTH Aachen University, Schinkelstr. 3, 52062 Aachen, Germany

ARTICLE INFO

Keywords:
B calcium-silicate-hydrate
B characterisation
B microstructure
E mortar
C shrinkage
B ^{1}H nuclear magnetic resonance

ABSTRACT

Moisture transport into concrete and mortar surfaces strongly influences the durability of structures. Transport processes are foremost controlled by the material's porosity. Cementitious materials, such as concrete and mortars, exhibit distinct changes in pore structure while drying and subsequent rewetting due to the internal shrinkage and swelling of the layered calcium-silicate hydrates.

Mortars with different w/c-ratios and binders were dried and rewetted and the subsequent time dependent changes in water filled pore structure were monitored with single-sided ^{1}H nuclear magnetic resonance. This technique combines a localized depiction of all pore water with a good time resolution. The NMR signal is split into the four pore species C-S-H interlayer water, gel pore water, interhydrate water, and capillary water by multi-exponential analysis. Two consecutive running processes in the swelling of cementitious mortars were identified and discussed based on recent models of the cement microstructure as well as its implications on the sorptivity.

1. Introduction

1.1. Pore structure of cementitious materials

On its smallest scale, cement stone is made up of hydrated calcium-silicates (C-S-H), being responsible for cohesion and strength. C-S-H forms the structural backbone and largely defines the pore structure. In this, gel pores form with sizes as small as a few nanometres. These pores strongly interact with water. Drying of gel pores leads to a shrinkage of cement stone and conversely, if empty gel pores are filled again, a swelling of the cement matrix occurs. [1–5] A currently widely adopted model developed by Jennings describes C-S-H as a lammenar [6] colloid [7] structure. This model is based on a composition of so-called globules with sizes of about 8 nm. Water is found in four different positions inside the globular C-S-H structure: (i) as so-called interlayer water between C-S-H sheets, (ii) in intraglobular pores (IGP) smaller than 1 nm, both inside the C-S-H globules, as well as (iii) in small gel pores (SGP) with sizes of about 1–3 nm and (iv) large gel pores (LGP) with sizes of 3–12 nm in interstitial spaces between globules. Within this model, large gel pores show similarities to capillary pores to some extent. IGP originate in imperfections inside the C-S-H sheets. Though being similar in size to small gel pores between globules, they largely differ in their accessibility to e.g. nitrogen, leaving voids upon emptying. In Fig. 1 a schematic representation of the pore spaces according to Jennings colloid model CM-II is drawn.

The detailed nature of the on-going processes while drying and rewetting in cement stone has been a point of discussion for some time. Mostly, two different processes at drying of hardened white cement paste are distinguished [3]: (i) mesopores grow between a relative humidity[1] (RH) of 95% down to 40%, accessible to both, water vapour and nitrogen and (ii) drying below 40% RH leads to the further increase of mesopore volume, interpreted as a consolidation of C-S-H structure. In the latter, differences in nitrogen and water vapour absorption are explained by nitrogen inaccessible IGP formed inside the consolidated C-S-H globules. Maruyama et al. [3] showed a temporary reduction of drying shrinkage between these processes, explained as resolution of capillary tension inside the pore structure. Similar results were obtained by Setzer and his co-workers before [4, 5].

On a slightly larger scale, capillary pores are formed by an excess of liquid water at the making as well as water emptied pore space due to chemical shrinkage and self desiccation [8]. These pores are associated with transport processes such as capillary sorption. The equations developed by Washburn [9] suggest, that sorptivity S is proportional to the porosity Φ times the square root of the overall transport effective pore radius R [10]. For simplicity, the contact angle between the wetting liquid and the pore surface α usually is set to zero, thus its influence

* Corresponding author.
E-mail address: schulte@ibac.rwth-aachen.de (R. Schulte Holthausen).

[1] Relative humidity in this context is defined as percent ratio of the partial pressure of water vapor to the equilibrium vapor pressure of water at a given temperature.

https://doi.org/10.1016/j.cemconres.2018.05.021
Received 9 March 2018; Received in revised form 9 May 2018; Accepted 30 May 2018

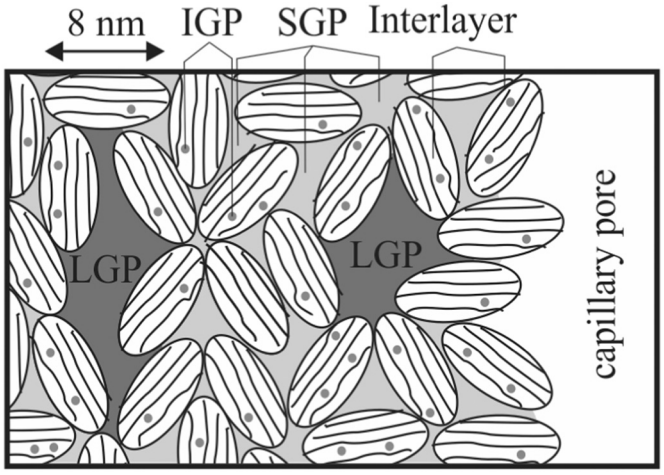

Fig. 1. Schematic representation of the C-S-H structure and water binding based on the CM-II model [6, 7]. The model is based on reoccurring units called globules. The model incorporates interlayer water, intraglobular pores (IGP), small gel pores (SGP), and large gel pores (LGP).

neglected [10, 11]. The overall curvature, described by tortuosity, and the interconnection of pores, described by restrictivity, are also expected to be important influences [10].

1.2. ^{1}H nuclear magnetic resonance on cementitious materials

One particularly insightful way for detecting moisture inside porous building materials is the use of ^{1}H nuclear magnetic resonance (NMR). This technique allows the quantification of moisture as well as an identification of different pore species. A high frequency electromagnetic pulse excites hydrogen nuclei, thereby causing a measurable response which is subsequently exponentially relaxing with time. The frequency of the excitation pulse needs to be matched with the inherent nuclei spin-frequency, which depends on the strength of the surrounding magnetic field. Heterogeneities in the magnetic field cause changes in spin-frequency and thereby a dephasing of the spins, leading to faster relaxation. Dephasing, caused by a constant heterogeneity, can be countered by certain pulse sequences, such as the well-known Carr-Purcell Meiboom-Gill (CPMG) sequence [12, 13], generating a series of rephasing echoes. This echo response is usually described by an exponential function with an amplitude at time zero and a relaxation time, describing the exponential decay over time. The amplitude can be directly and linearly correlated with the gravimetric water content [14], as long as all water causing the gravimetric change is detected by the NMR method. This might not be the case for hydrogen showing a rather fast relaxation, such as solid portlandite and ettringite crystals [15], C-S-H interlayer [16], or even gel pore water [11]. Furthermore, different pore species can be distinguished by their volume to surface ratio and therefore by their relaxation times [15, 17, 18].

Systematic and extensive research on fully and partly saturated cement stone only recently enabled the attribution of relaxation times to certain pore water species [14, 15, 19]. Working with a NMR frequency of 20 MHz in an enclosed magnet setup on white cement pastes, five essential pore species were found. They were assigned to (i) water in solid crystals such as portlandite and ettringite,[2] (ii) to water inside the lamellar C-S-H structure, (iii) to water inside C-S-H gel pores, (iv) to smaller interhydrate pores and (v) larger capillary pores being a remnant of hydration. The corresponding relaxation times are ~0.01 ms, ~0.1 ms, ~0.4 ms, ~1 ms, and ~10 ms respectively. Such relaxation times change to some extent with the frequency of the spectrometer used, with the amount of paramagnetic impurities such as Fe_2O_3 in the material [17], as well as with the saturation degree of the pores. Based on the fast exchange model, a direct conversion from relaxation times to pore size has been developed [20], that lately has been shown to give comparable results to other porosity measurement techniques, such as mercury intrusion porosimetry [21].

Concerning the swelling of C-S-H gel during capillary uptake experiments, Rucker-Gramm and Beddoe [11] used NMR in combination with other methods. They illustrated that a deviation from the square root-law at sorption experiments is directly related to a decrease of NMR amplitude. This is caused by the conversion of water in larger capillary pores to water in smaller and faster relaxing gel pores. The latter was not visible for the device used. These effects were dependent on the initial water content, beginning at the first wetted surface, further processing inside the material. Fischer et al. [16] used a different NMR setup and illustrated the rearrangement of water from large capillaries to smaller gel pores directly by NMR. Due to the device used, not all pore species inside the cement pore structure were detected. Recently, an enclosed magnet setup was used for experiments on C-S-H shrinkage and subsequent swelling [22]. To overcome the need for spatial resolution, cement paste was crushed to pieces of several millimetres and wetted as granules. They found irreversible changes only to happen during the initial drying cycle and that a more severe drying process leads to considerably more rearrangement of porosity. Concerning the differentiation of the two subsequently happening processes while drying described as above, they observed a close relationship between growth of finer porosity and reduction of coarser porosity and concluded, that the two processes mirror each other and represent the opposite sides of the same process. In Fig. 2, the time dependent change in the porosity of a sample of hardened white cement paste with a w/c-ratio of 0.4, dried at 60 °C under slightly reduced pressure und subsequently rewetted is shown, data taken from Gajewicz et al. [22]. Here, the continuous refinement of porosity can clearly be seen. The very first signal of the redeveloping gel pores appear after 8 h. In their study, a reduced emphasis was put on the timescale of the ongoing processes, especially the very first moments after rewetting with the very first measurement conducted after 2 h.

The present study uses a single-sided ^{1}H nuclear magnetic resonance device allowing a highly localized spatial depiction of all the pore species involved with a good temporal resolution.

2. Experiments

2.1. Materials

Mortars made from two different cements, one ordinary Portland cement (OPC) as well as one blast furnace slag cement (BFC) according to DIN EN 197-1:2011, mixed with sand according to DIN EN 196-1:2016 were used. Table 1 gives the composition of the cements. The mortars were prepared according to DIN EN 196-1:2016 and the mix designs are shown in Table 2. Minor segregation between water and the sand-cement mixture for higher w/c-ratios was observed during production.

After mixing the mortars were cast in prisms with dimensions of $40 \times 40 \times 160\,mm^3$, left in the mouldings for two days and subsequently cured at > 95% RH for 28 days. Following, the prisms were cut to small plates of 10 mm thickness with a water-cooled diamond saw.

2.2. Methods

After sample preparation, two separate experiments were conducted. First, samples were characterised in saturated and dried state by single-sided ^{1}H NMR for their moisture dependent pore volumes. Another set of samples was dried and rewetted and the continuous change in NMR signal was recorded to monitor the time-dependent swelling of pore structure. Afterwards, such samples were investigated by NMR for irreversible changes in pore structure. In Fig. 3 the workflow of the experiments is depicted.

[2] Only visible by NMR through a so-called solid echo sequence.

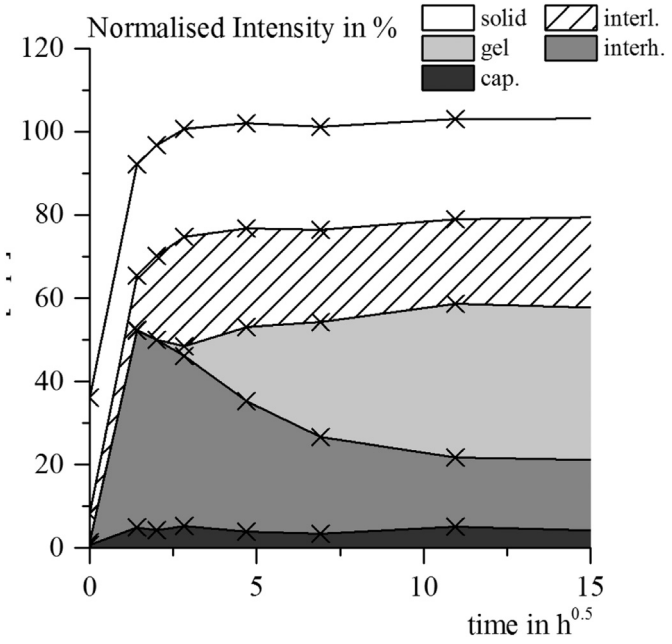

Fig. 2. NMR signal intensity over time, normalized to the maximum value obtained, showing the time-dependent change in porosity of hardened white cement paste with a w/c-ratio of 0.4, dried at 60 °C under slightly reduced pressure. Data obtained from Gajewicz et al. [22].

Table 1
Cement composition according to DIN EN 196-2:2013.

Contents	CEM III/A 32.5 N-LH	CEM I 52.5 R
	wt%	
Portland cement clinker	51.1	90.7
Granulated slag	42.2	0.0
Limestone	2.9	3.9
Setting regulator (sulphate)	3.8	5.4
Na_2O	0.32	0.26
MgO	3.45	0.74
Al_2O_3	7.91	3.70
SiO_2	27.30	22.00
SO_3	3.79	3.36
K_2O	0.54	0.47
CaO	52.80	65.80
TiO_2	0.56	0.21
MnO	0.16	0.04
Fe_2O_3	1.46	1.30

Table 2
Mortar mix design.

Cement	w/c-ratio	Cement	Sand
–	–	g	
CEM III/A 32.5 N-LH	0.4	550	1350
	0.5[a]	450	
	0.6	375	
	0.7	315	
CEM I 52.5 R	0.4	550	
	0.7	315	

[a] Standard mortar mixture for cement testing according to DIN EN 196-1:2016.

For characterisation, two samples of each mortar were first saturated at atmospheric pressure (1 bar) for about 14 days and subsequently dried at 40 °C and 105 °C,[3] for about 28 and 7 days, respectively. Every saturation and drying storage was kept until a constant mass ($\Delta m < 0.01$ wt%/d) was reached. After every step samples were weighed and measured by single-sided NMR for a more precise porosity characterisation. Furthermore, the saturated sample's volume was measured by immersion weighing to convert gravimetric to volumetric results. For the more precise porosity characterisation, a profile with five depths between 1.2 and 2.0 mm inside the sample was measured with 1024 scans in each depth. The results of five depths were averaged to increase the signal to noise ratio and to cover a larger, more representative volume of the sample.

For NMR measurements of time-dependent changes of pore structure, one sample of each mortar was dried at 40 °C and 105 °C until a constant mass was reached. Before further experiments, they were stored in an unregulated desiccator for a maximum duration of one week to prevent an excess of moisture or CO_2 to come in contact with the samples. For the experiments, samples were placed on the NMR device for a first dry measurement. After this, a thin felt was laid into a specially prepared thin petri dish filled with tap water and together placed on the sensor. The sample was placed inside the petri dish, first slightly tilted to prevent air from being trapped underneath the sample, and then brought to rest horizontally. The continuous NMR measurement, in a depth of roughly 1 mm inside the sample, was started instantaneously. Measurements were performed continuously over at least the initial 8 h. Afterwards, samples were stored under water and taken out for measurements in increasing time intervals over 28 days. During the first hour, measurements with 128 consecutive scans were averaged, giving roughly one relaxation decay per minute. Afterwards 1024 scans were averaged, each lasting approximately 8.5 min. Fig. 4 illustrates the measurement setup. After completion of swelling, the samples were measured by NMR in five depths between 1.2 and 2.0 mm, comparable to the measurements of precise porosity characterisation.

All NMR measurements were carried out with a single-sided NMR MOUSE PM5 (Nuclear Magnetic Resonance Mobile universal surface explorer Profile Mouse 5 mm), developed and manufactured by the Institute of Macromolecular Chemistry of the RWTH Aachen University [23]. While such devices can nowadays be acquired from Magritek GmbH, Germany, the device used is an early prototype using a minispec MQ20 spectrometer from Bruker cooperation. The NMR MOUSE uses a sophisticated array of permanent magnets, generating a well-levelled layer as the measurement field. This sensitive volume has dimensions of roughly $20 \times 20 \times 0.2\,mm^3$, allowing the non-destructive assessment of high-resolution hydrogen profiles through the surface of materials up to a depth of 2 mm. A CPMG sequence was applied with a total of 1000 echoes and an echo time T_E of 0.03 ms, using the parameters in Table 3.

2.3. Data evaluation

For data evaluation, echo amplitudes were normalized by the amplitude of pure water A_W, measured with a sufficient waiting time between subsequent scans of 20 s. Furthermore, the first two echoes were corrected for transient effects [24, 25] and a slight “spurious oscillation” [26] in the relaxation signal, which resulted in the normalized and corrected signal amplitude A_c/A_W. In the following, this corrected and normalized NMR signal is called the NMR porosity Φ_{NMR}. Exponential decays were evaluated by curve fitting with four independent exponential components using a least-squares algorithm:

[3] The drying chambers were standing in a surrounding laboratory climate of 23 °C and 65% RH. On the assumption of constant absolute air water content, relative drying temperatures would correspond with a RH of 26% and 2% at 40 and 105 °C respectively.

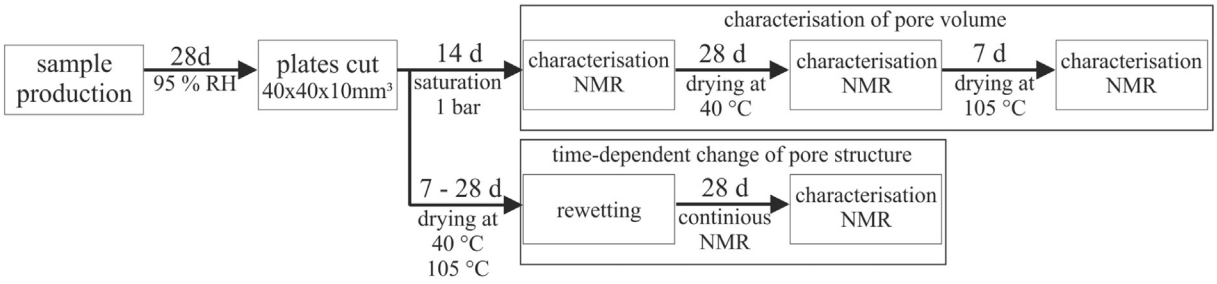

Fig. 3. Workflow of the experiments.

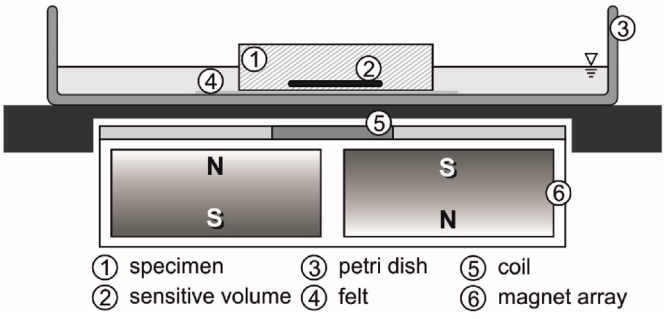

Fig. 4. Setup for single-sided NMR measurements of internal swelling.

Table 3
NMR measurement parameters used.

Parameter	Value	Unit
Magnetic field gradient	21.6	T/m
Measurement frequency	18.15	MHz
Recycle delay	500	ms
Echo-spacing T_E	30	µs
Pulse-length	4.5	µs
Acquisition window	5	µs
Number echoes	1000	–
Number scans	128/1024	–

$$F(t) = \sum_{n=1}^{4} A_n \exp\left(-\frac{t}{T_{2-n}}\right)$$

Here, *F (t)* is the echo value of CPGM-Fit at time *t*, *n* is the number of the fit component, *t* is the time, A_n is the fitted amplitude and $T_{2\text{-}n}$ is the fitted relaxation time. Values for relaxation times were limited between three times the echo time T_E and the T_2-relaxation time of pure water due to diffusive attenuation [27, 28], thus between 0.09 ms and 115 ms. Furthermore, the individual relaxation times were limited between three times the next shorter and one third of the next longer relaxation time, to prevent overlapping. The comparatively low signal to noise ratio of the continuous NMR measurements demanded a different approach, since a fit with eight free values lead to distorted results. To be able to better compare the results, all relaxation times were fixed, based on the more precise characterisation measurement. This selection of relaxation times is addressed further in the discussion. A full comprehensive description of the experiments can be found elsewhere [29].

3. Results

The results of the NMR signals for porosity characterisation measurements are given in Fig. 5 and the corresponding T_2-relaxation times in Table 4. For the measurement of saturated samples, the four fitting components A_1 to A_4 are shown. The corresponding relaxations times T_2 are around 0.12, 0.4, 1.5 and 10 ms respectively, matching earlier results in the literature [15, 22]. In the following, they are interpreted as the four signal components of (A_1) interlayer water bound in dense

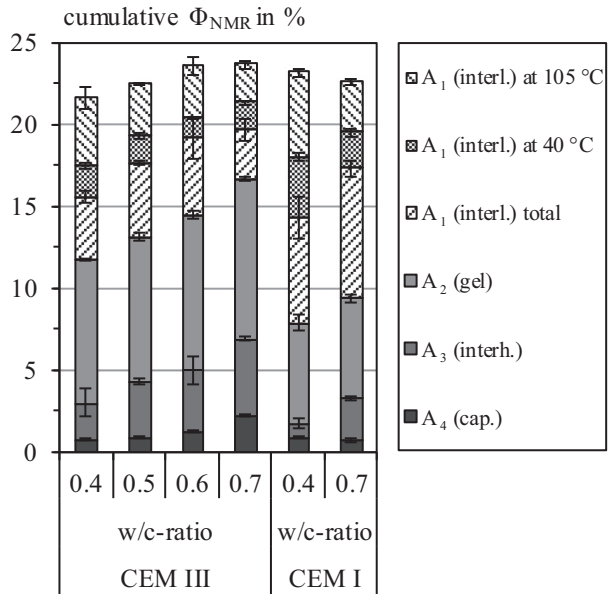

Fig. 5. Results from NMR characterisation measurement of the amplitudes for saturated mortar samples and an age of 35 days; NMR signal amplitudes are split into four components in dependence of their corresponding relaxation times T_2 in Table 4 and furthermore, according to the signal remnants after drying at 40 and 105 °C.

Table 4
T_2-relaxation times for the mortar samples obtained from characterisation measurement.

Cement	w/c-ratio	T_{2-1} (interl.)	T_{2-2} (gel)	T_{2-3} (interh.)	T_{2-4} (cap.)
–	–	ms			
CEM III	0.4	0.121	0.40	1.34	9.2
	0.5	0.132	0.43	1.46	8.9
	0.6	0.137	0.50	1.76	8.3
	0.7	0.140	0.49	1.85	9.8
CEM I	0.4	0.098	0.30	1.15	7.3
	0.7	0.137	0.44	1.55	6.0

calcium silicate hydrate (C-S-H) sheets, (A_2) water bound in small gel pores around 2 nm in size, (A_3) water in so-called interhydrate pores (~10 nm), and (A_4) water in larger capillaries (> 10 nm) respectively. It has been shown before that a continuous drying empties pores consecutively, starting from the larger capillaries proceeding to the smaller pores [20]. When drying at 40 or 105 °C, most pore spaces are emptied completely and even the signal of C-S-H interlayer water is decreased considerably [22]. Therefore, in Fig. 5 the signal of interlayer water is split into the remnants after 105 °C drying, additional remnants after 40 °C drying and total signal of C-S-H interlayer water, which is measured upon complete saturation.

With increasing w/c-ratio, an increase in interhydrate and capillary

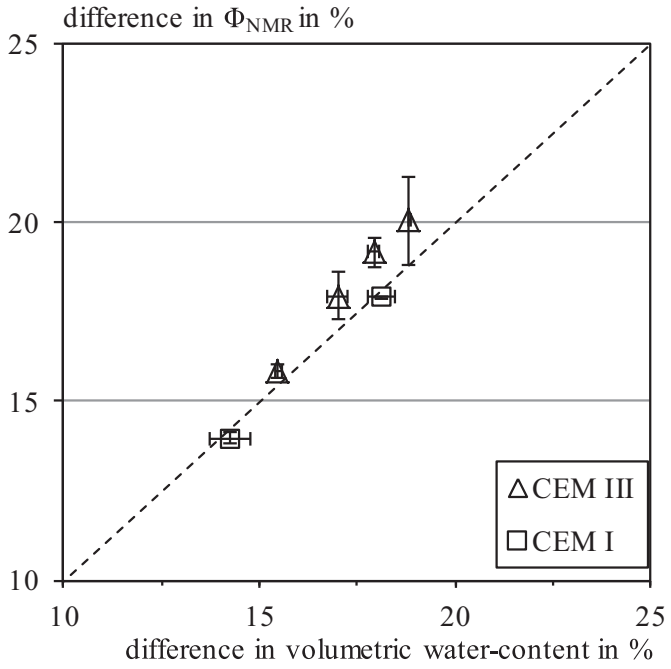

Fig. 6. Difference in volumetric water content and NMR amplitudes Φ_{NMR} for samples saturated at atmospheric pressure and dried at 40 °C.

porosity can be observed. Furthermore, the amount of gel porosity is almost independent of the w/c-ratio. Lastly, the amount of signal in dense C-S-H is decreasing with increasing w/c-ratio which is expected due to the reduced amount of cement in the mix. In general, this matches the original predictions for porosity composition of Powers [8], though absolute numbers might differ due to a different hydration degree or an influence of aggregates. Signal remnants after drying are considerably increased for mortars with lower w/c-ratios, indicating a slightly coarser pore-structure for higher w/c-ratio and a denser pore structure for low w/c-ratio. On average, 3% more C-S-H interlayer water is evaporated at 105 °C compared to 40 °C. Larger differences occur between mortars made with BFC and OPC. The amount of C-S-H interlayer water for OPC is considerably larger than for BFC. This is surprising to some extent, since BFC containing cements are reported to develop an overall denser structure [30]. Though having had the same age, the samples might have had a different degree of hydration due to the slower reaction of BFC, as also indicated by the remnants of water after drying. Nonetheless, we found similar differences between OPC and BFC for well-hydrated samples too.

Fig. 6 depicts the change in volumetric water content between saturation and drying at 40 °C compared to the difference in the corresponding NMR signal. The results show a direct and linear correlation between the NMR signal Φ_{NMR} and the volumetric change on drying. The deviations from the diagonal are most likely caused by heterogeneities in the samples as well as minor drying dependent changes in mass, not visible to the NMR technique employed. Furthermore, differences in the signal might by influenced by binder inherent features as well as the data evaluation by multi-exponential fitting. Further insight into the pore structure of mortars and concretes incorporating different binders might be obtained by more complex inverse Laplace transformation on more comprehensive data sets, though beyond the scope of this publication. Nonetheless, with the comparatively small deviations from the diagonal line shown, the NMR signal can be regarded as the volumetric water content, comparable to results of other porous materials and similar single-sided NMR devices before [31].

The results of time dependent porosity NMR measurements of selected mortars dried at 40 and 105 °C are shown in Fig. 7. For the temporal analysis, relaxation times were set according to Table 4. In the first hour, a stronger variation in amplitudes arises due to the reduced amount of scans in this period accompanied by a lower signal to noise ratio. In the following, we first concentrate on samples dried at 40 °C. In the first minute after rewetting, water fills the pore system with the total signal amplitude reaching almost 80% of the final value after only four minutes (0.25 √h). With a steep initial increase, first, only coarse capillary and interhydrate porosity is filled. Within 15 min the signal associated with the coarsest capillary pores as well as some interhydrate pore volume is replaced by signal associated with gel pore spaces. For mortars with a w/c-ratio of 0.5 and below, little to no coarse capillary porosity is remaining. Interestingly, the increase of gel pores in the first hour is accompanied by a temporary reduction of C-S-H interlayer water. Finally, interhydrate spaces are further diminished by the growth of first mostly gel spaces, followed by the growth of interlayer C-S-H in a much slower reaction, continuing over the whole 28 days of the measurement. While OPC binders generally reveal similar effects, the late growth of C-S-H is even more prominent.

For mortars dried at 105 °C the initial filling of coarse pores with water happens even faster. At the same time, a delayed increase of C-S-H interlayer spaces occurs. Gel pore spaces are completely abundant in the first hour after rewetting. Furthermore, the initial increase of gel porosity is happening delayed, though as well accompanied by a reduction of C-S-H interhydrate spaces. For samples with a low w/c-ratio, this process happens after 24 h. For higher w/c-ratio samples it is happening at increased times, for a w/c-ratio of 0.7 after 48 h.

The mortar sample made with BFC and a w/c-ratio of 0.4 dried at 105 °C experiences a low point in coarsest pores at around 64 h (8 √h). This was caused by a temporarily loss of water in the petri dish while prolonged continuous measurement, causing a drying of the largest pores. After the subsequent immersion in water, this low point vanishes, the largest pores are filled again.

The results of the characterisation measurement after drying, rewetting, and completion of swelling after > 40 days are shown in Fig. 8. To be able to better compare the results with the results of the samples as prepared (never dried), the same T_2-relaxation times, given in Table 4, were used and only changes compared to the results from samples as prepared are shown. Positive values indicate an increase, negative a decrease of such signal. Symmetry of positive and negative results indicate an unchanged overall signal. While some overall trends are visible, the results indicate a certain amount of scattering. For all samples, an overall reduction of coarse pores, capillary and interhydrate spaces, as well as an increase in finer porosity, gel or interlayer spaces, is found. Samples dried at 105 °C rather show an increased gel porosity, BFC samples dried at 40 °C an increase in C-S-H interlayer water. All in all, a slight decrease in porosity is found for samples dried at 40 °C of about 1%. Such change is not seen for samples exposed to 105 °C.

4. Discussion

4.1. Reversible changes while rewetting

The detailed nature of the on-going processes while drying and rewetting has been a point of discussion for some time. This study sheds further light on the complex processes of moisture dependent porosity changes while rewetting. For reference, we aim to base the following descriptions on the terms and concepts of the colloid-model II [6]. Fig. 9 depicts the overall changes in C-S-H structure and swelling processes as discussed below. Drying at 40 °C empties gel pores, resolves capillary forces, and partly consolidates the C-S-H micro structure. Due to the shrinking forces, gel pores partly open and form larger expanded gel pore spaces (EGP) and partly shrink to consolidated gel pore spaces (CGP). Drying at 105 °C leads to an almost complete consolidation of gel pores though not increasing the overall porosity. The shrunken gel pore space does not differ considerably from C-S-H interlayer water as seen in NMR.

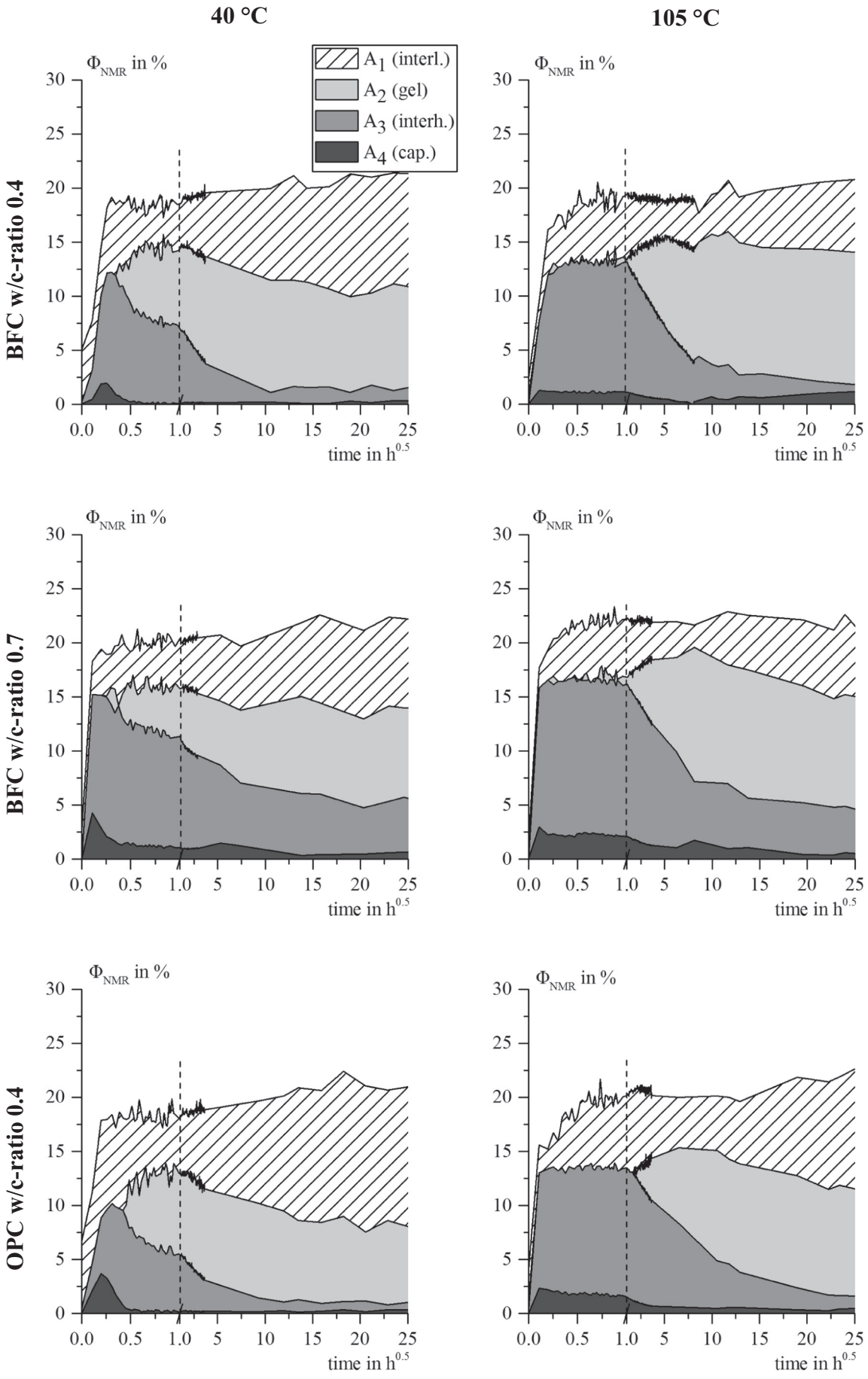

(caption on next page)

Fig. 7. Change in NMR signals after drying at 40 °C (left) and 105 °C (right) subsequently rewetting for mortar with BFC w/c 0.4 and 0.7 and OPC w/c 0.4. Four pore species are shown: C-S-H interlayer water (hatching), gel water (light grey), interhydrate water (medium grey) and capillary water (dark grey). Results are presented on a square root of time axis split at 1 h into two different scalings.

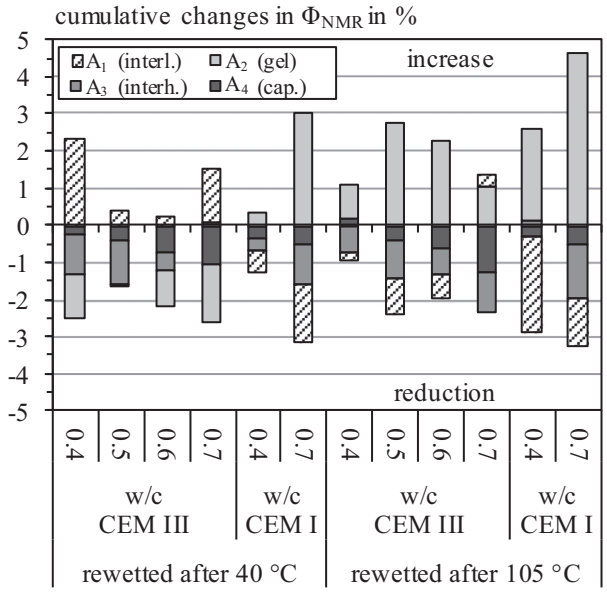

Fig. 8. Results from NMR characterisation measurement of the changes in amplitude, after 40 °C drying and 40 days after rewetting and after 105 °C drying and 50 days after rewetting. Saturation by atmospheric pressure; NMR signal amplitudes are split into four components, in dependence of their corresponding T_2-relaxation times. Positive values indicate an increase, negative a decrease of such signals. Symmetry of positive and negative values indicates an unchanged overall signal intensity.

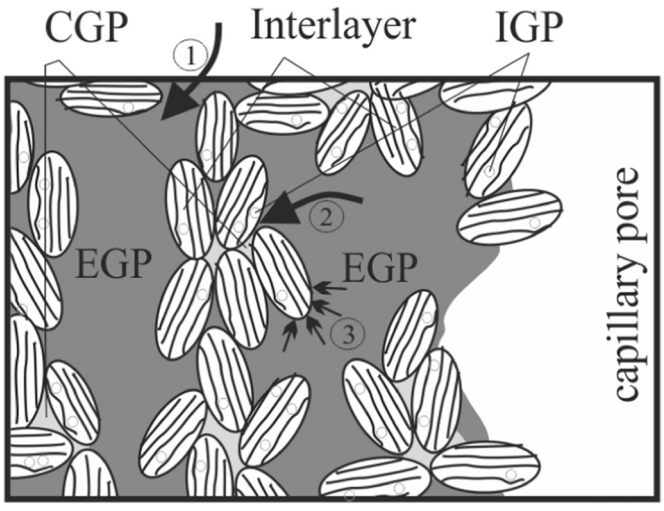

Fig. 9. Schematic representation of the restructuring of dried C-S-H globules including consolidated gel pores (CGP) and expanded gel pores (EGP). Upon rewetting, water (1) almost instantaneously floods the available open pore space and (2) reinvades gel pore space, if not fully consolidated. In a third (3), considerably slower process, water ingresses into C-S-H interlayers and IGP.

Upon rewetting a mortar, previously dried at 40 °C, first, all open spaces are reinvaded almost instantaneously due to capillary forces. Second, gel pore spaces, decisively shrunk though not entirely fused together, are re-invaded in a process running for up to 15 min. A temporary decrease of C-S-H interlayer signal appears due to dried up gel pore spaces quickly growing to their original size in the fast swelling process. Third, the re-entry into consolidated C-S-H interlayer spaces as well as intraglobular pores on the other hand is a considerably slower process, overcoming the strong joining forces. For samples, dried at 105 °C and rewetted, gel space is strongly consolidated to condensed C-S-H sheets. Water molecules re-entering into the original C-S-H interlayer as well as consolidated gel pore spaces have to overcome the strong surface joining forces before the consolidated gel spaces can be expanded again. The re-invasion becomes a tedious, long lasting process running for several weeks.

Surprisingly, the first value for the coarsest capillary porosity is higher for mortars dried at 40 °C and lower for mortars dried at 105 °C. With a more severe drying process, one would expect an even coarser porosity. One possible explanation is the reduction of the coarsest pores after 105 °C in an even faster time scale after rewetting, not even resolvable with the procedure employed here. Another influence might be the ionic concentration inside the pore solution, changing NMR relaxation without considerate change in pore structure [21]. However, it might be questioned, why the samples dried at different temperatures should react considerably different in this regard. Furthermore, recent results comparing hardened white cement paste dried at 50 and 100 °C with mercury intrusion porosimetry did as well show a minimally increased coarse porosity for samples dried at 50 °C compared to a drying at 100 °C [21].

The results obtained in this study differ to some extent from the results reported in the literature [22], as well outlined in Fig. 2. While putting more emphasis on the first hour after rewetting, the results here show an increase in C-S-H interlayer water, not seen in Fig. 2. The choice of relaxation times for the different pore types influence the outcome of the results. Assigning a different relaxation time, for example a relaxation time assigned to C-S-H that is closer to the range of gel water, will lead to a C-S-H signal in NMR, mimicking gel pore behaviour. Fixed relaxation times were chosen in this study, which likely caused at least some mimicking behaviour of pore types. On the other hand, assuming a constant surface relaxivity of the samples, at least for samples incorporating the same binder, allows direct comparison of pore sizes and pore size changes.

4.2. Irreversible changes due to drying

The overall loss of coarse porosity due to drying, shown in Fig. 7, is in accordance with the CM-II model, indicating irreversible shrinkage [6], though recent results in the literature [22] did report opposite effects. Differences between these and our findings might be due to the prolonged duration of our experiments of > 40 days between rewetting and testing. In shorter durations, the swelling process might not have come to an end. As well, some further hydration of the BFC samples investigated here might have taken place during the drying and rewetting. It is, however, not entirely clear if the loss in signal of the coarsest pores is as well influenced by an insufficient saturation of ink-bottle pores by capillary processes. In a recent study, only minor changes in degree of saturation were found for samples, saturated at atmospheric pressure compared to a saturation with 200 bar [21], which would presumably fill such pores. More accurate measurements in enclosed magnet setups as well as measurements of macroscopic shrinkage might give further insight.

Drying cementitious materials at temperatures as high as 105 °C poses severe stress on the pore structure. In a recent study [30], the development of microcracks (1 to 60 µm width) due to comparable severe drying was investigated on paste, mortar, and concrete samples. Such cracks might well be an influence on the values in capillary porosity seen in our experiments, though, a permanent distinctive rise of coarse porosity due to micro cracking as previously reported for

concrete heated to even higher temperatures [32] has not been found. If the NMR signal A_4 is related to the filling of microcracks, the reduction and near disappearance of this signal might as well give some indication, why only comparatively small effects of microcracks were found in the study while drying was said to pose a superior role in transport properties. Microcracks, prominent in a dried state, close when samples are rewetted.

4.3. Implications on sorptivity of cementitious materials

Keeping in mind that sorptivity is largely influenced by porosity and overall pore size, a strong impact of the described changes in porosity on the sorptivity is expected. The reinvasion of partly consolidated pore space lasting for roughly 10 min would most likely be only noticeable between the start of any capillary water uptake testing and first weighing. Such short time anomaly has been reported [33]. The longer lasting process might induce deviation from simple square root time behaviour over a duration of 12 to 36 h, depending on drying temperature and material mixture [34].

Concerning the change rate of interhydrate porosities after roughly 1 h, an almost linear curve over a square root of time axis can be observed. This agrees well with the recent arguments by Villagran Zaccardi et al. [34]. They suggested a sorptivity function of cementitious materials based on the fourth root of time. They argued, that such behaviour is best explained, if changes in pore structure followed a square root of time function. Such is indeed seen here. Capillary ingress [9] as well as diffusive transport [35] both would explain such square root of time ingress behaviour. However, it should be noted, that other functions such as exponential or stretched exponential behaviour [36] fit equally well the results presented.

5. Conclusions

In this study, dried mortar samples have been rewetted and the change in porosity has been continuously monitored using single-sided ^{1}H nuclear magnetic resonance. The relaxation signals have been interpreted and assigned to four different pore species [14, 19]. The following conclusions are drawn:

- Single-sided nuclear magnetic resonance allows the characterisation of water bound in cementitious mortars and with it, the characterisation of porosity. It is not necessary to determine the absolute water content of samples by drying. Other than previously used enclosed magnet setups, this allows investigation of the porosity of heterogeneous samples or samples not suitable for enclosed magnet setups.
- Upon drying, a considerable amount of water bound in C-S-H interlayer spaces is evaporated. Looking closer at the porosities immediately after rewetting, a reduction of fine pore space is seen up to a drying temperature of 40 °C causing the opening of larger cavities. At 105 °C, C-S-H interlayer water is further emptied. No further open porosity volume is developed, though C-S-H interlayers are further consolidated.
- After rewetting of mortars dried at 40 °C, three processes happen simultaneously, though seen subsequently in the measurements. First, water reinvades empty pores immediately. Second, a fast reinvasion of beforehand shrunk gel pores causes swelling and reduces the overall coarser porosity. Third, a much slower reinvasion of consolidated C-S-H interlayer spaces proceeds over several weeks, further reducing gel and capillary pore space. In mortars dried at 105 °C, gel pores are consolidated to an extent that no fast swelling is observed.
- Links between the results of porosity change here and the change in sorptivity in capillary water uptake experiments have been drawn, that will be further addressed in future experiments. Altogether, based on ours and recent findings in the literature [30] the role of drying and its influence on transport properties and the durability of concrete structures might be worth investigating further.

Acknowledgement

The authors would like to thank the German Technical and Scientific Association for Gas and Water, grand no. W-5-01-14, for funding the project.

References

[1] R.F. Feldman, P.J. Sereda, A model for hydrated Portland cement paste as deduced from sorption-length change and mechanical properties, Mater. Constr. 1 (1968) 509–520.
[2] R.F. Feldman, P.J. Sereda, A new model for hydrated portland cement and its practical implications, Engl. J. (1970) 53.
[3] I. Maruyama, Y. Nishioka, G. Igarashi, K. Matsui, Microstructural and bulk property changes in hardened cement paste during the first drying process, Cem. Concr. Res. 58 (2014) 20–34.
[4] C. Duckheim, M.J. Setzer, Hygric properties of hardened cement paste, in: M.J. Setzer (Ed.), Transport in Concrete: Nano- to Macrostructure: TRANSCON 2007, Aedificatio Publishers, Freiburg, 2007, pp. 217–226.
[5] M.J. Setzer, A. Liebrecht, The properties of pores solution in hardend cement paste, in: M.J. Setzer (Ed.), Transport in Concrete: Nano- to Macrostructure: TRANSCON 2007, Aedification Publishers, Freiburg, 2007, pp. 207–215.
[6] H. Jennings, Refinements to colloid model of C-S-H in cement: CM-II, Cem. Concr. Res. 38 (2008) 275–289.
[7] H. Jennings, A model for the microstructure of calcium silicate hydrate in cement paste, Cem. Concr. Res. 30 (2000) 101–116.
[8] T.C. Powers, Structure and physical properties of hardened portland cement paste, J. Am. Ceram. Soc. 41 (1958).
[9] E.W. Washburn, The dynamics of capillary flow, Phys. Rev. 17 (1921) 273–283.
[10] D. Benavente, P.G.D.C. Lock, A.S. Ordonez, Predicting the capillary imbibition of porous rocks from microstructure, Transp. Porous Media 49 (2002) 59–76.
[11] P. Rucker-Gramm, R.E. Beddoe, Effect of moisture content of concrete on water uptake, Cem. Concr. Res. 40 (2010) 102–108.
[12] H.Y. Carr, E.M. Purcell, Effects of diffusion on free precession in nuclear magnetic resonance experiments, Phys. Rev. 94 (1954) 630–638.
[13] S. Meiboom, D. Gill, Modified SpinEcho method for measuring nuclear relaxation times, Rev. Sci. Instrum. 29 (1958) 688–691.
[14] A. Gajewicz, Characterisation of Cement Microstructure and Pore–Water Interaction by 1H Nuclear Magnetic Resonance Relaxometry, Department of Physics, University of Surrey, 2014.
[15] P.J. McDonald, V. Rodin, A. Valori, Characterisation of intra- and inter-C-S-H gel pore water in white cement based on an analysis of NMR signal amplitudes as a function of water content, Cem. Concr. Res. 40 (2010) 1656–1663.
[16] N. Fischer, R. Haerdtl, P.J. McDonald, Observation of the redistribution of nanoscale water filled porosity in cement based materials during wetting, Cem. Concr. Res. 68 (2015) 148–155.
[17] R. Valckenborg, NMR on Technological Porous Materials, Eindhoven University, Eindhoven, 2001.
[18] W.P. Halpering, J. Jehng, Y. Qiao Song, Application of spin-spin relaxation to measurement of surface area and pore size distribution in a hydrating cement paste, Magn. Reson. Imaging 12 (1994) 169–173.
[19] A. Muller, Characaterization of Porosity & C-S-H in Cement Pastes by H-NMR, Eidgenössische Technische Hochschule Lausanne, Lausanne, (2014).
[20] A. Muller, K. Scrivener, A. Gajewicz, P. M., Use of bench-top NMR to measure the density, composition and desorption isotherm of C-S-H in cement paste, Microporous Mesoporous Mater. 178 (2013) 99–103.
[21] A. Muller, K. Scrivener, A reassessment of mercury intrusion porosimetry by comparison with 1H NMR relaxometry, Cem. Concr. Res. 100 (2017) 350–360.
[22] A. Gajewicz, E. Gartner, K. Kang, P. McDonald, V. Yermakou, A 1H NMR relaxometry investigation of gel-pore drying shrinkage in cement pastes, Cem. Concr. Res. 86 (2016) 12–19.
[23] B. Blumich, J. Perlo, F. Casanova, Mobile single-sided NMR, Prog. Nucl. Mag. Res. Sp. 52 (2008) 197–269.
[24] M.D. Hurlimann, Diffusion and relaxation effects in general stray field NMR experiments, J. Magn. Reson. 148 (2001) 367–378.
[25] F. Casanova, J. Perlo, B. Blümich, Single-Sided NMR, Springer, 2011.
[26] P. McDonald, A. Gajewicz, R. Morrell, National Physical Laboratory Good Practice Guide No. 144 - The Characterisation of Cement Based Materials Using T2 1H Nuclear Magnetic Resonance Relaxation Analysis, NPL Management Limited, United Kingdom, 2016.

[27] D.G. Rata, F. Casanova, J. Perlo, D.E. Demco, B. Blumich, Self-diffusion measurements by a mobile single-sided NMR sensor with improved magnetic field gradient, J. Magn. Reson. 180 (2006) 229–235.
[28] M.D. Hurlimann, D.D. Griffin, Spin dynamics of Carr-Purcell-Meiboom-Gill-like sequences in grossly inhomogeneous B(0) and B(1) fields and application to NMR well logging, J. Magn. Reson. 143 (2000) 120–135.
[29] L. Kling, On the Influence of Internal Swelling on the Porosity, the Capillary Water Uptake, and the Electrical Conductivity in Mortars, Institute of Building Materials Research, RWTH Aachen University, Aachen, 2018 (unpublished).
[30] Z. Wu, H.S. Wong, N. Buenfeld, Transport properties of concrete after drying-wetting regimes to elucidate the effects of moisture content, hysteresis and microcracking, Cem. Concr. Res. 98 (2017) 136–154.
[31] B. Blumich, S. Anferova, R. Pechnig, H. Pape, J. Arnold, C. Clauser, Mobile NMR for porosity analysis of drill core sections, J. Geophys. Eng. 1 (2004) 177–180.
[32] R. Schulte Holthausen, O. Weichold, Non-destructive evaluation of thermal spalling in concrete by single-sided nuclear magnetic resonance, ASNT J. Infrastruct. Syst. 23 (2016).
[33] D.A. Lockington, J.Y. Parlange, Anomalous water absorption in porous materials, J. Phys. D. Appl. Phys. 36 (2003) 760–767.
[34] Y. Villagran Zaccardi, N. Alderete, N. De Belie, Improved model for capillary absorption in cementitious materials: progress over the fourth root of time, Cem. Concr. Res. 100 (2017) 153–165.
[35] J. Crank (Ed.), The Mathematics of Diffusion, second ed., Clarenndon Press, Oxford, 1975.
[36] J.B. Hubbard, T. Nguyen, D. Bentz, A model of defect-mediated transport through amorphous membranes, J. Chem. Phys. 96 (1992) 3177–3182.